Numerical assessment of wave induced loads on an Oscillating Water Column carapace

M. Batlle Martin, Grégory Pinon, J. Reveillon

Numerical assessment of wave induced loads on an Oscillating Water Column carapace

M. Batlle Martin & G. Pinon
LOMC, UMR 6294, CNRS - Normandie Univ. UNIHAVRE, 76600 Le Havre, France

J. Reveillon
CORIA, UMR 6614, CNRS - Normandie Univ. UNIROUEN, 76000 Rouen, France

ABSTRACT: This paper aims to describe preliminary work guidelines for the survivability study of Oscillating Water Column (OWC) using computational fluid dynamics. OpenFOAM has been used to analyse, first, the feasibility to reproduce an irregular sea state. Historical data from a near-shore buoy on Saint-Jean-de-Luz has been used for this purpose. Seconds, an Oscillating Water Column large scale geometry has been tested on a hydrostatic imbalance hydrodynamic situation. Finally, the OWC structure at the end of a large scale numerical wave flume has been studied facing a near-shore irregular sea state. Strengths and weaknesses regarding the numerical tool performance are presented and settle a point of departure to reproduce more storm events.

1 INTRODUCTION

The actual climate debate has focused on energy generation and more precisely, on efficiency and feasibility of large devices producing clean energy at a national level. This green energy dependency evokes the importance of a diversified and versatile system to fulfil the dynamic population needs. Through this current, there is a rising part of the population that highlights the great source of clean energy that oceans could provide. The variety of cyclic processes occurring at oceans, such as tidal, thermal currents, or water waves, makes evident this rising interest. Nevertheless, these phenomena may be an opportunity or an issue. In terms of waves, large waves can cause important damages and losses in the coastlines due to their highly energetic impacts (Quevauviller et al. 2017), or conversely, they can be seen as a huge source when looking at their potential energy properties. Therefore, we can take advantage of these two facts together in a technical way by installing wave energy devices onto coastal protection structures. Oscillating Water Column (OWC) is a possible concept (Falcão and Henriques 2016), protecting the shoreline and generating clean energy at the same time. This engineering structure has been already tested in Toftestallen (Norway), Sakata harbour (Japan), Pico Island in Acores (Portugal) (Neumann and Crom 2011), (Falcão et al. 2020), Mutriku (Spain) (Torre-Enciso et al. 2009) or in Limpet, Islay (UK). Multiple studies have focused on these kind of device from an experimental point of view e.g. (Gouaud et al. 2010), (Allsop et al. 2014), or using different numerical approaches; (Delauré and Lewis 2003), (Dimakopoulos et al. 2015), (Elhanafi et al. 2016), among others. Experiences from OWC prototypes deployments has, however, shown that it is easy to underestimate wave loading on such devices (Medina-Lopez et al. 2015). Direct wave loads have been a matter of interest for many years, (Bagnold 1939), (Hattori et al. 1994) or (Bullock et al. 2007), and reasonably good prediction methods are available, e.g; Goda (2010). But these are proposed and validated for simple structures like caisson breakwaters and they need to be adapted for more complex structures as the OWC. Here the oscillating behaviour between the interior and the exterior fluid can lead to undesired stress on the structure carapace. Furthermore, the overturning of some waves during an irregular sea state leads to impulsive loads on the exposed part of the structure. This paper aims to give insights on these matters using the Computational Fluid Dynamics (CFD) approach utilising the open-source numerical toolbox OpenFOAM. It is the continuation of a previous work where the same numerical tool was used and validated against experiments in determining waves impact pressure peaks. Other studies have also employed successfully this numerical tool for

similar purpose e.g. (Liu et al. 2019), (Hu et al. 2017) or (Ferrer et al. 2016). The present work is organised in four sections, where; firstly, the numerical model core equations are presented. Secondly, an irregular sea state is reproduced numerically on deepwater conditions with a flat bottom. Next, a mesh sensitivity and a qualitative analysis of the structure undergoing a fluid oscillation problem are studied in Section 4. Finally, the structure is evaluated facing an irregular sea state with a subsection highlighting an impulsive event.

2 NUMERICAL TOOL

In this section, the numerical model assumptions and core equations are introduced. A multiphase solver is chosen using a finite volume spatial discretisation and Volume Of Fluid (VoF) to track the free surface between phases, namely; air and water. The Navier-Stokes equations ensure the momentum conservation at every cell, taking the form:

$$\frac{\partial \rho \mathbf{u}}{\partial t} + \nabla \cdot (\rho \mathbf{u}\mathbf{u}) = -\nabla p_d - \mathbf{x} \cdot \mathbf{g} \nabla \rho + \mu \nabla^2 \mathbf{u} \,, \quad (1)$$

where ρ is the phase density, $\mathbf{u}$ is the cell centred velocity vector, $p_d = p - \rho \mathbf{x} \cdot \mathbf{g}$ is a relative modified pressure introducing a density gradient near the interface and $\mu = \rho\nu$ the dynamic molecular viscosity, ν is the kinematic viscosity. The problems presented in this scope are assumed to be inertial driven flows and, thus, the surface tension effects is neglected for the sake of simplicity. A laminar model has been employed in this paper. Secondly, to ensure the mass conservation the continuity equation takes the general form:

$$\frac{\partial \rho}{\partial t} + \nabla \cdot (\rho \mathbf{u}) = 0 \,. \quad (2)$$

In order to model two phases a new variable, namely liquid volume fraction α, is introduced as:

$$\alpha = \frac{\rho - \rho_{air}}{\rho_{water} - \rho_{air}} \,, \quad (3)$$

taking values of 1 for water and 0 for air. The liquid volume fraction transport equation, using a Multidimensional Limiter for Explicit Solution (MULES, see for instance Deshpande, Anumolu, & Trujillo (2012)), for a compressible flow reads:

$$\frac{\partial \alpha}{\partial t} + \nabla \cdot (\alpha \mathbf{u}) = -\frac{\alpha}{\rho} \left(\frac{\partial \rho}{\partial t} + \mathbf{u} \nabla \rho \right) \,, \quad (4)$$

where the right-hand side of the equation takes into account the compressibility effects.

The barotropic equations of state (EOS) are introduced for both phases as:

$$p + p^* = (\gamma - 1) e \rho \,, \quad (5)$$

Table 1: Buoy details extracted from the CANDHIS websiste

Buoy reference	06403
Observation time frame	6 years
Latitude	43°24,500'N
Longitude	01°40,900'N
Depth [m]	20
Tidal range [m]	3.75

where γ is the specific heats ratio and e is the internal energy per unit mass. Last equation (5) presents a modification of the standard EOS for perfect gas $p = (\gamma - 1)\rho e$ first presented by Cole (1948) in his study of *Underwater explosions* by adding the constant p^* which depends on the phase speed of sound. The assumption of barotropic fluids allows the possibility of not solving the energy equation, increasing the computational speed.

3 IRREGULAR SEA STATE

In this section, the objective is to reproduce numerically an irregular sea state and analyse the possible limitations. It is modelled, initially using a Join North Sea Wave Observation Project JONSWAP spectrum as a wind-wave fully developed sea using significant wave height H_s and the peak period T_p parameters. A peak enhancement factor of 3.3 is employed. The calibration of the spectrum is based on real data from CANDHIS (Centre dArchivage National de Donnes de Houle In Situ, Conseil Général des Pyrénées Atlantiques et CEREMA (2020)) regarding the buoy located $1.2\,km$ away from Saint-Jean-de-Luz (see Table 1).

A rectangular numerical domain of $150\,m$ long and $30\,m$ high without any obstacle (no OWC device at this stage) is used to model a 2D configuration of a wave flume. An orthogonal structured mesh is employed for the spatial discretisation with a geometric vertical grading refinement close to the interface. An initial water depth of $20\,m$ is chosen according to the buoy conditions. The boundary conditions are defined as; open for the top edge, a wall for the bottom, an absorbing boundary at the end of the numerical wave flume, and a static wave generation for the inlet as the left boundary.

This type of inlet imposes velocities and free surface elevation following the chosen wave theory. Here the irregular theory employs a linear superposition of first order Stokes waves for a given number of components N_s, where the free surface is calculated as:

$$\eta(x,t) = \sum_{i=1}^{N_s} \frac{H_i}{2} cos(k_i x - \omega_i t + \psi_i) \,. \quad (6)$$

Here H_i is the wave height, k_i the wave number, ω_i the angular frequency and ψ_i the wave phase. Similarly, the velocities are calculated using a superposition of the linear theory for every wave.

The most probable sea-state at the buoy location, with $H_s = 1\,m$ and $T_p = 9\,s$, is first tested. The input spectrum frequencies only range from $f_p/2$ to $3\,f_p$ to be representative, and the number of components is $N_s = 500$. Figure 1 presents the results obtained for this sea-state conditions in terms of spectral density and frequency after $t = 15\,min$, $t = 30\,min$ and $t = 60\,min$. The results are extracted from a numerical gauge located $10\,m$ away from the wave generator recording free surface elevation at every $t = 0.5\,s$. The spectral density is estimated from the temporal series using the Welch's method (Welch 1967) by averaging over 12 periodograms spectrums estimates.

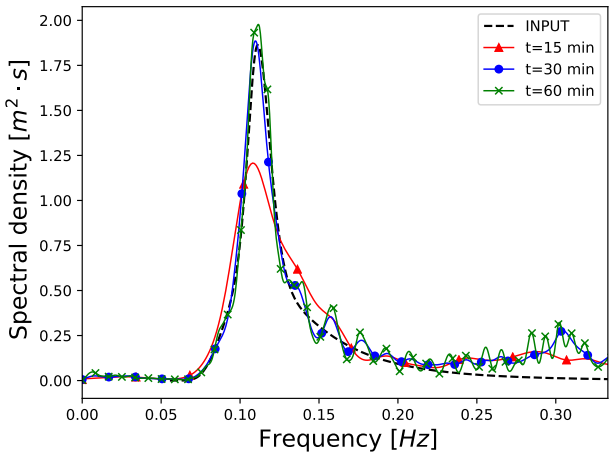

Figure 1: Developing spectrum, $H_s = 1\,m$ and $T_p = 9\,s$.

A fairly good agreement is found in terms of peak frequency and shapes for these sea-state conditions. The physical time length is a key parameter to fully develop the irregular sea state, which, in this situation is achieved after $t = 30\,min$. Smaller wave periods, from $T \leq 5\,s$ or $f \geq 0.2\,Hz$, are over estimated here. This could be caused by some reflection from the outlet absorbing boundary, which is meant to be more suitable for shallow water conditions. Extracted from the free surface temporal series, a significant wave height $H_s = 1.1\,m$ is obtained and an $H_{max} = 2.15\,m$. Obtaining fairly good results only $10\,m$ away from the wave generator allows using such small domain to reproduce this kind of irregular sea state assuming there is no wave reflection. The simulation was run in parallel over 4 processors and it took $9\,h$ to simulate $15\,min$ physical time.

4 THE OSCILLATING PROBLEM

This section focuses on a qualitative analysis of the Oscillating Water Column working behaviour in a simplified case. The geometry of the structure was reproduced from (Medina-Lopez et al. 2015) and represents the device located in Mutriku. The work presented in this Section aims to model the incoming waves run-up and run-down process together with the structure response. The fluid starts from a static position where there is a hydrostatic difference Δh between the inside and the outside of the chamber, see

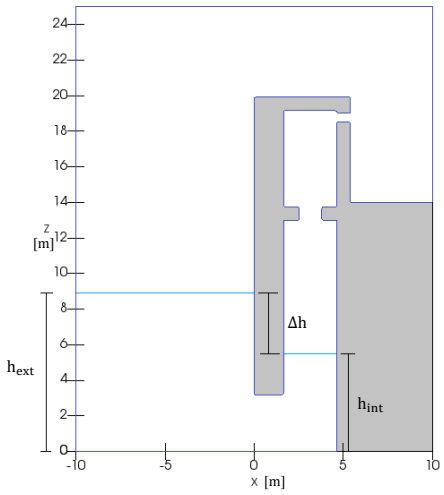

Figure 2: Oscillating water column device sketch

Fig. 2. After the initialisation, the water is flowing inside the chamber raising the h_{int} level and pushing the air out of the structure. Once the interior free surface reaches the highest level the water will flow now out from the chamber pulling air inside the structure, and so forth. This test case was chosen because it is based on the geometry used for the following of the paper. Several other test-cases exist in the literature such as (Delauré and Lewis 2003, Zhang et al. 2012) and they may be used as a matter of further validation of the numerical software shortly.

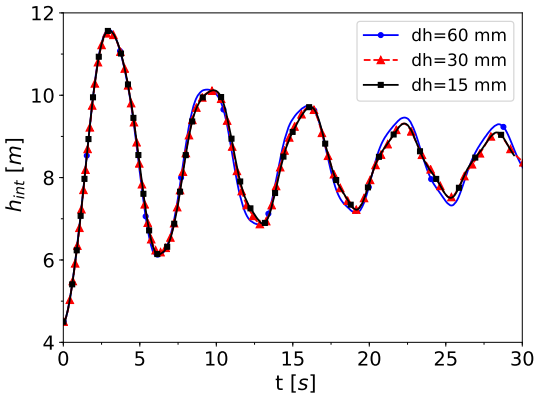

Figure 3: Free surface elevation convergence inside the chamber for 3 different mesh discretisations

Figure 3 depicts some results of the convergence study carried out setting with $h_{int} = 4.5\,m$ and $\Delta h = 5\,m$. The free surface elevation inside the chamber is plotted against time for three different mesh refinements. The cell size for the finest mesh is $dh = 15\,mm$. A good convergence is achieved for all three discretisations during the first oscillation. Next, the coarser mesh slightly miss-predict the free surface behaviour, while, the finest meshes are superposed one another.

During the study of (Medina-Lopez et al. 2015), it was mentioned the importance of the carapace lower part geometry, which may induce pressure drops and, eventually, cavitation. During the first oscillation, the flow entering the chamber close to the carapace edge creates a recirculation zone, which drops the pressure

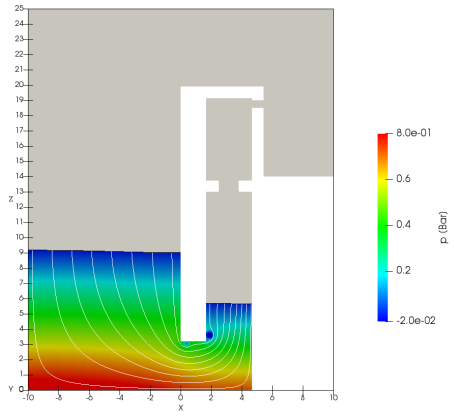

Figure 4: Pressure fields and streamlines at $t = 0.7\,s$

as it is observable in Figure 4.

5 OSCILLATING WATER COLUMN ANALYSIS

In this section, a real scale Oscillating Water Column device is modelled facing an irregular sea state. Both the irregular sea-state (Section 3) and the OWC device (Section 4) are put together to analyse the behaviour of the structure. The OWC geometry employed here is the same as in Fig. 2 and is placed on the right-hand side of a $152\,m$ long and $47\,m$ high 2D domain. The channel has $30\,m$ long of horizontal sea-bed, where the irregular sea state can develop. Next, a typical South West Atlantic bathymetry with a slope of 7% represents the near-shore in front of the structure. The employed mesh has 176.000 cells and is mostly orthogonal with some triangular cells in the vicinity of the sloped plane (see Figure 5). The interface region has a uniform cell aspect ratio of $dx = 2 \cdot dy$ and a cell height of $dy = 0.125\,m$. Above and below this region, the mesh has a geometric grading in the vertical direction. The structure is covered by two consecutive refinements in both orthogonal directions. The boundary conditions are defined as open for the top edge, a wall for the bottom and the structure, and a static wave generation for the inlet introducing an irregular sea state (see eq.(6)).

The simulation presented in this section 5 were all performed using a maximum Courant number of 0.65. Second-order or blended schemes were employed for spatial discretisation scheme. The time derivatives were solved using second-order schemes, except the liquid volume fraction time derivative, for which a first-order bounded scheme was used. Using the computing resources provided by CRIANN (Centre Régional Informatique et d'Applications Numériques de Normandie), the simulation was run in parallel over 56 processors and it approximately took $23\,h$ to simulate $750\,s$ of physical time.

5.1 *Normal sea-state in front of the carapace*

With this configuration, the so called normal conditions spectrum with $H_s = 1\,m$ and $T_p = 9\,s$ (see Fig. 1), were tested for two water depth conditions, representing two different tidal levels. At low tide, the structure carapace is submerged $0.8\,m$, a value which increases to $4.55\,m$ for high tide. During the study of (Medina-Lopez et al. 2015), it was highlighted the fact that the most damaged caissons were those without any turbine installed. For this reason, in the present study, the location of the turbine is kept empty assuming the less favourable situation for the OWC. Figure 6 shows the obtained results for low tide conditions, regarding a pressure temporal series on the front face of the carapace. In this series, the pressure ranges within hydro-static and dynamic values, without any relevant impulsive event. Following the recommendations by (Bullock et al. 2007), these waves are referred to as *slightly-breaking* as the maximum pressure recorded remains lower than 2.5 the maximum quasi-hydrostatic pressure in this location. Using the formulas proposed by Goda (2010) for *wave pressure under wave crests*, the maximum pressure on the sea water level (SWL) is $p_1 = 0.18\,bar s$. This value corresponds to a $H_{max} = 1.8\,H_s$ and slightly overestimates the obtained results.

Regarding the temporal pressure series (Fig. 6), a high value is reached at $t = 359\,s$. This wave event is further studied in Figure 7. Starting at $t = 357.5\,s$ with an even water level inside and outside the chamber, the incoming wave approaches. The studied wave, when it is $5\,H_s$ far from the carapace, has an approximate wave height of $1\,m$. As the wave starts the run-up phase, the free surface inside the chamber rises slightly slower. The pressure profiles on the inner face of the carapace depict a drop of pressure close to the bottom edge caused by a recirculation zone.

On the other hand, while using the same irregular spectrum $H_s = 1\,m$ and $T_p = 9\,s$, now with high tide conditions, the pressure signal at the SWL $Z = 7.75\,m$ is presented in Figure 8. Increasing the water depths h, the ratio H/h decreases leading to a less probable situation of waves breaking. Regarding the formula proposed by Goda (2010) for pressure on the SWL, the α_1 there presented decreases as the water depth increases. Thus, higher water depths predict lower pressure values conversely as it is presented in Figure 8 compared to Figure 6. This fact may be related to resonance between the incoming waves and the oscillatory behaviour inside the chamber, which may amplify the waves run-up on the structure. Further analysis should be carried out on this line for the sake of better perspectives.

5.2 *Identification of a wave impact on the carapace*

In this section, the same irregular sea state has been employed but the water depth on the structure has decreased to $h = 3.4\,m$, representing a very low tide (near the lowest astronomical tidal value). And thus, only $0.2\,m$ of the carapace is submerged initially. These conditions will propitiate the presence of wave

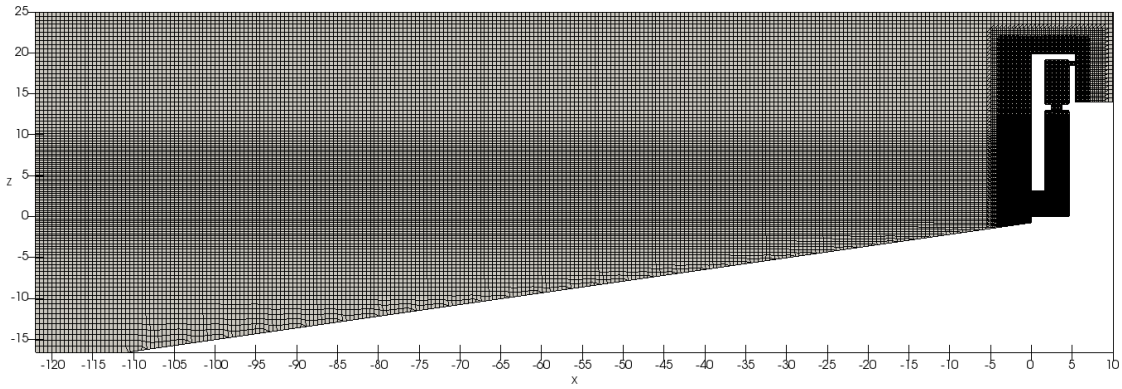

Figure 5: Numerical domain

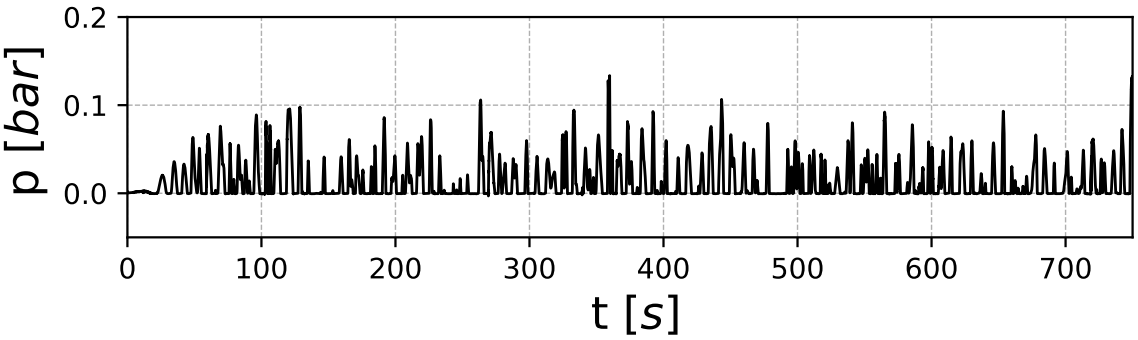

Figure 6: Sea water level pressure serie on the carapace front face for low tide conditions ($h = 4\,m$)

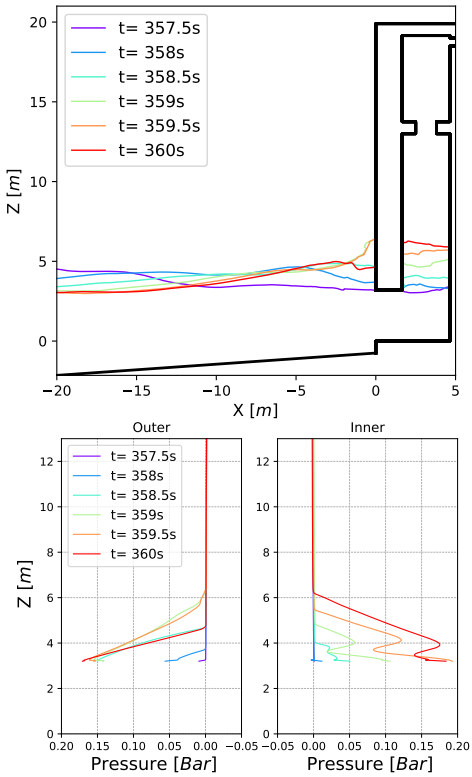

Figure 7: Low tide conditions - Top: Free surface. Bottom: Pressure profiles on the front and the back face of the carapace

breaking or the airflow through the bottom of the carapace.

Testing these conditions, a relevant event has been observed, as presented in Figure 9. Here, the run-down process has reduced the water depths on the vicinity of the structure leaving the carapace surrounded by air. As the next incoming wave approaches, the free surface rises fast and rapidly impacts the bottom face of the carapace and, finally, at $t = 134.95\,s$ (see Fig. 9), a splash phenomenon occurs.

Recording the pressure values on a point located at the carapace bottom face during this event, the pressure signal presented in Figure 10 is obtained. Values up to $0.3\,bar$ are observed combined with a sudden pressure rise during $\Delta t \approx 50\,m\,s$ approximately. This pressure peak is followed by compressibility effects, as the recorded pressure oscillations denote, and a pressure plateau during the splash phenomenon. This pressure peak exceeds the maximal pressure records on the SWL (see Figures 6 and 8) and is caused by a random wave during the most probable irregular state situation. This precise configuration with an impulsive event may not be extremely critical to the structure. But, from the few test-cases run so far, it showed that such a phenomenon may be reproduced and identified via the presented numerical procedure. Finally, at present, the agitated configurations are still under consideration with the addition of a relaxation zone close to the wave maker (left of the domain, see Fig. 5) to dampen the reflected waves. Once validated, many more configurations representing the full wave conditions based on the scatter diagram and represen-

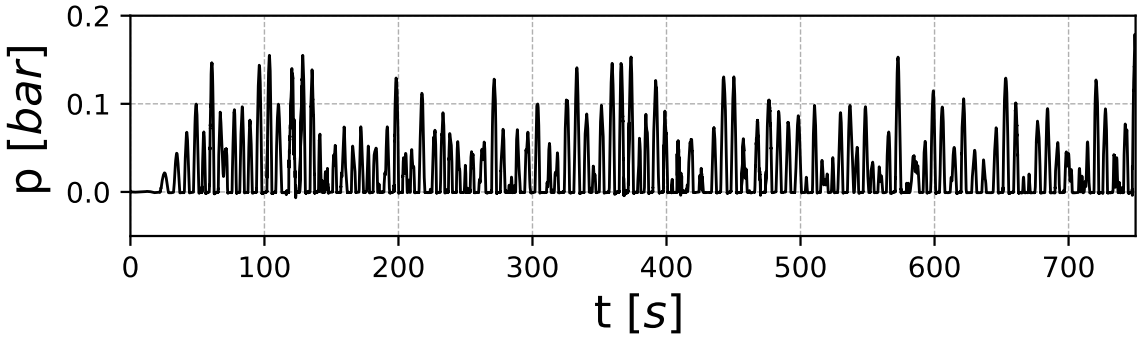

Figure 8: Sea water level pressure serie on the carapace front face for high tide conditions ($h = 7.75\,m$)

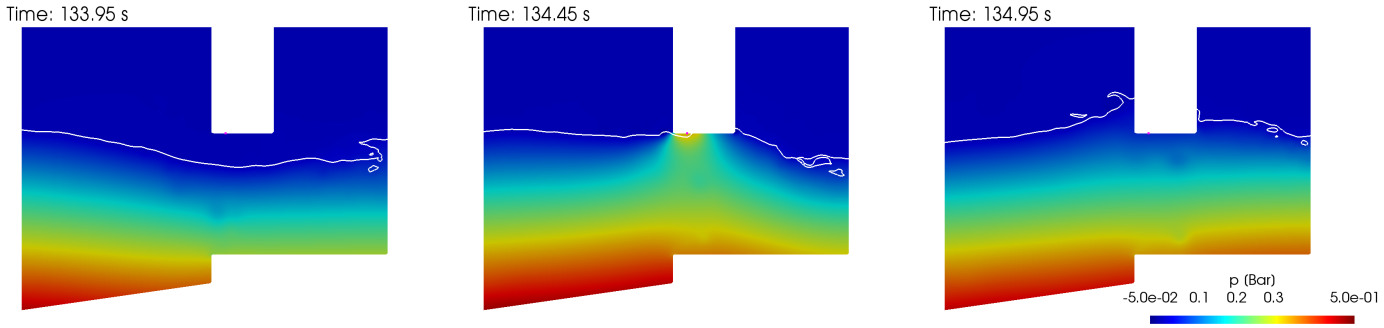

Figure 9: Identification of a wave impact on the bottom of the carapace

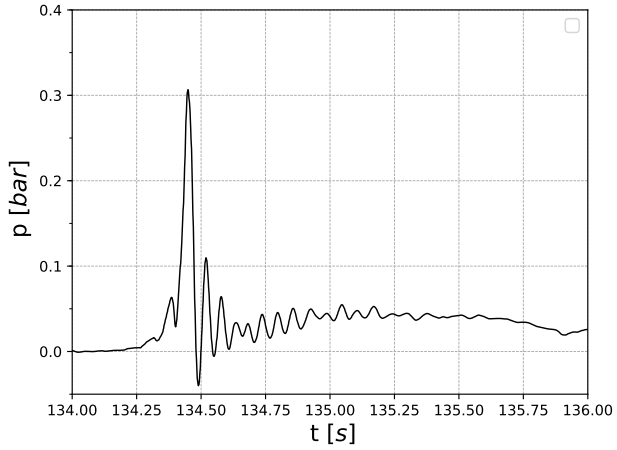

Figure 10: Relative pressure signal on the carapace bottom face

tative tidal levels will be run to investigate the most critical conditions.

6 CONCLUSIONS

A preliminary methodology to numerically evaluate peak impact pressures onto the carapace of an Oscillating Water Column was presented and detailed. The studied configuration is based on the Mutriku OWC geometry applied in the Saint-Jean-de-Luz region. The numerical tool is the Computational Fluid Dynamics code OpenFOAM, which is open-source software and used in a 2D compressible formulation. The CFD tool was first employed to evaluate its capabilities to reproduce different irregular sea states conditions, following a JONSWAP distribution. Secondly, the Mutriku full-scale OWC geometry was tested on an oscillatory flow induced by a hydrostatic pressure difference between the interior and exterior of the chamber. From previous studies, the shape of the lower carapace has been identified as an important point of design as it may induce recirculation zones. Such a recirculation zone was also observed in our numerical computations. These first tests gave promising results, which will be completed by additional test-cases from the literature. Finally, the OWC geometry has been tested facing irregular waves. The full-scale geometry was immersed in a larger domain to investigate the pressure series recorded on the carapace with a normal sea-state.

Pressure records on the carapace for slightly-breaking waves are in good agreement with the literature. Furthermore, an impulsive event on the lower part of the carapace highlighted the importance of the water depths in front of the structure. Although the full software procedure is now in a good way to be validated, several simulations of agitated to extreme irregular sea-states are now envisaged to investigate the survivability conditions of such wave energy devices installed on coastal protection structures. Several computations based on the wave scatter diagram (H_s, T_p) will be run to fully represents the wave conditions encountered in the Saint-Jean-de-Luz region. Also as a perspective, different turbulence models are under investigation as well as a simplistic approach to take into account the presence of a turbine, following the recommendations presented on (Dimakopoulos et al. 2015). This will lead to an assessment of the Damage Equivalent Loads to better design the structure.

7 ACKNOWLEDGEMENTS

M. Batlle Martin acknowledges the financial support for his PhD grant from the regional council of Normandie. The authors acknowledge the financial support of the CPER-ERDF program DIADEMAR funded by the Normandy Regional Council and the European Union. The present work was performed on computing resources provided by CRIANN (Normandy, France). The authors acknowledge the financial support of the Agence Nationale de la Recherche, through the program Investissements davenir - LabEx EMC3 via the project PERCUSS.

REFERENCES

Allsop, W., T. Bruce, J. Alderson, V. Ferrante, V. Russo, D. Vicinanza, & M. Kudella (2014, 08). Large scale tests on a generalised oscillating water column wave energy converter.

Bagnold, R. A. (1939). Interim report on wave-pressure research. *Journal of the Institution of Civil Engineers 12*(7), 202–226.

Bullock, G., C. Obhrai, D. Peregrine, & H. Bredmose (2007). Violent breaking wave impacts. part 1: Results from large-scale regular wave tests on vertical and sloping walls. *Coastal Engineering 54*(8), 602 – 617.

Cole, R. H. (1948). *Underwater explosions.* Princeton,Princeton Univ. Press,.

Conseil Général des Pyrénées Atlantiques et CEREMA (2020). Fiches synthétiques de mesure des états de mer du réseau candhis. http://candhis.cetmef.developpement-durable.gouv.fr.

Delauré, Y. & A. Lewis (2003). 3d hydrodynamic modelling of fixed oscillating water column wave power plant by a boundary element methods. *Ocean Engineering 30*(3), 309 – 330.

Deshpande, S. S., L. Anumolu, & M. F. Trujillo (2012, nov). Evaluating the performance of the two-phase flow solver interFoam. *Computational Science & Discovery 5*(1), 014016.

Dimakopoulos, A., M. Cooker, E. Medina-Lopez, D. Longo, & R. Pinguet (2015, 09). Flow characterisation and numerical modelling of owc wave energy converters.

Elhanafi, A., A. Fleming, G. Macfarlane, & Z. Leong (2016). Numerical energy balance analysis for an onshore oscillating water columnwave energy converter. *Energy 116*, 539 – 557.

Falcão, A. F. & J. C. Henriques (2016). Oscillating-water-column wave energy converters and air turbines: A review. *Renewable Energy 85*, 1391 – 1424.

Falcão, A. F., A. J. Sarmento, L. M. Gato, & A. Brito-Melo (2020). The pico owc wave power plant: Its lifetime from conception to closure 19862018. *Applied Ocean Research 98*, 102104.

Ferrer, P. M., D. Causon, L. Qian, C. Mingham, & Z. Ma (2016). A multi-region coupling scheme for compressible and incompressible flow solvers for two-phase flow in a numerical wave tank. *Computers and Fluids 125*, 116 – 129.

Goda, Y. (2010). *Random Seas and Design of Maritime Structures* (3rd ed.). WORLD SCIENTIFIC.

Gouaud, F., V. Rey, J. Piazzola, & R. V. Hooff] (2010). Experimental study of the hydrodynamic performance of an onshore wave power device in the presence of an underwater mound. *Coastal Engineering 57*(11), 996 – 1005.

Hattori, M., A. Arami, & T. Yui (1994). Wave impact pressure on vertical walls under breaking waves of various types. *Coastal Engineering 22*(1), 79 – 114. Special Issue Vertical Breakwaters.

Hu, Z. Z., T. Mai, D. Greaves, & A. Raby (2017). Investigations of offshore breaking wave impacts on a large offshore structure. *Journal of Fluids and Structures 75*, 99 – 116.

Liu, S., I. Gatin, C. Obhrai, M. C. Ong, & H. Jasak (2019). Cfd simulations of violent breaking wave impacts on a vertical wall using a two-phase compressible solver. *Coastal Engineering 154*, 103564.

Medina-Lopez, E., W. Allsop, A. Dimakopoulos, & T. Bruce (2015). *Conjectures on the Failure of the OWC Breakwater at Mutriku*, pp. 592–603.

Neumann, F. & I. L. Crom (2011, 5-9 Sep. 2011). Pico owc - the frog prince of wave energy? recent autonomous operational experience and plans for an open real-sea test centre in semi-controlled environment. In *9th European Wave and Tidal Energy Conference (EWTEC)*. Southampton, UK.

Quevauviller, P., P. Ciavola, & E. Garnier (2017). *Xynthia, February 2010: Autopsy of a Foreseable Catastrophe*, Chapter 3, pp. 111–148. John Wiley & Sons, Ltd.

Torre-Enciso, Y., I. Ortubia, L. L. de Aguileta, & J. Marqués (2009, September). Mutriku wave power plant: from the thinking out to the reality. In *8th European Wave and Tidal Energy Conference (EWTEC)*. Uppsala, Sweden.

Welch, P. (1967). The use of fast fourier transform for the estimation of power spectra: A method based on time averaging over short, modified periodograms. *IEEE Transactions on Audio and Electroacoustics 15*(2), 70–73.

Zhang, Y., Q.-P. Zou, & D. Greaves (2012). Airwater two-phase flow modelling of hydrodynamic performance of an oscillating water column device. *Renewable Energy 41*, 159 – 170.